

# Spectroscopy and diode-pumped laser operation of Pr:LaMgAl<sub>11</sub>O<sub>19</sub> crystal

Shidong Zhou<sup>a</sup>, Yuxin Pan<sup>a</sup>, Nan Li<sup>b</sup>, Bin Xu<sup>b</sup>, Jian Liu<sup>a</sup>, Qingsong Song<sup>a</sup>, Jie Xu<sup>a</sup>, Dongzhen Li<sup>a</sup>, Peng Liu<sup>a</sup>, Xiaodong Xu<sup>a,\*</sup>, Jun Xu<sup>c,\*\*</sup>

<sup>a</sup> Jiangsu Key Laboratory of Advanced Laser Materials and Devices, School of Physics and Electronic Engineering, Jiangsu Normal University, Xuzhou, 221116, China

<sup>b</sup> Department of Electronic Engineering, Xiamen University, Xiamen, 361005, China

<sup>c</sup> School of Physics Science and Engineering, Institute for Advanced Study, Tongji University, Shanghai, 200092, China

## ARTICLE INFO

### Keywords:

Pr:LMA  
Czochralski method  
Spectral property  
Laser property

## ABSTRACT

We report on the growth, spectroscopic properties and visible laser operation of Pr<sup>3+</sup>-doped LaMgAl<sub>11</sub>O<sub>19</sub> (LMA) crystal. The absorption and emission spectra were recorded in visible wavelength range and the decay time of <sup>3</sup>P<sub>0</sub> manifold was measured to be about 34.5 μs at room temperature. Using an InGaN laser diode as pump source, continuous-wave laser operation of Pr:LMA crystal have also been demonstrated in red at about 645 nm and deep red at about 725 nm, which provide new linearly polarized sources for various potential applications.

## 1. Introduction

Visible lasers have attracted a great deal of attention due to their important applications, such as data storage, display technology, medical treatment and indoor optical communication [1,2]. Trivalent praseodymium (Pr<sup>3+</sup>) ions doped materials have proved to be attractive active media for visible laser output when excited by cheap and compact InGaN laser diodes [3–5]. They can offer various laser transitions from the <sup>3</sup>P<sub>0</sub> upper laser level into the lower lying manifolds. The corresponding emissions have been demonstrated in blue, green, orange, red and deep red spectral regions [6].

Up to now, a great deal of Pr<sup>3+</sup> lasers has been developed based on various host materials such as fluoride crystals LiYF<sub>4</sub> [7], LiGdF<sub>4</sub> [8], LiLuF<sub>4</sub> [9], KYF<sub>4</sub> [10], KY<sub>3</sub>F<sub>10</sub> [11], BaY<sub>3</sub>F<sub>8</sub> [12] LaF<sub>3</sub> [13], and CaF<sub>2</sub> [14], oxide crystals YAlO<sub>3</sub> (YAP) [15], LaMgAl<sub>11</sub>O<sub>19</sub> (LMA) [16], SrAl<sub>12</sub>O<sub>19</sub> (SRA) [17], CaAl<sub>11</sub>O<sub>19</sub> (CAIO) [18], and Sr<sub>0.7</sub>La<sub>0.3</sub>Mg<sub>0.3</sub>Al<sub>11.7</sub>O<sub>19</sub> (ASL) [19]. Fluoride crystals are good host materials for visible lasers due to their low phonon energies and comparably low crystal field strength, which prevent non-radiative decay of the <sup>3</sup>P<sub>0</sub> upper laser level and excited state absorption (ESA) to the 4f5d configuration [1]. Compared with fluoride crystals, oxide crystals possess better thermomechanical properties and can be easily grown by the Czochralski method. Unfortunately, many Pr<sup>3+</sup>-doped oxide crystals exhibit ESA in the visible spectral region. Nevertheless, several highly coordinated oxide host materials have been found to be suitable for visible lasers.

A very interesting system is the strontium hexa-aluminate

SrAl<sub>12</sub>O<sub>19</sub>, which has the magnetoplumbite structure PbFe<sub>12</sub>O<sub>19</sub> and the space group *P*6<sub>3</sub>/*mmc* [20–22]. The large divalent Sr<sup>2+</sup> cationic sites can be partially or totally substituted by La<sup>3+</sup> ions and charge compensation will be accomplished by Mg<sup>2+</sup> ions, which substitute the small trivalent host cations Al<sup>3+</sup> [23–25]. In Pr<sup>3+</sup>-doped crystals, Pr<sup>3+</sup> is supposed to substitute the twelfold coordinated Sr<sup>2+</sup>/La<sup>3+</sup> site. Because the Pr<sup>3+</sup> ions are exposed to a relatively weak crystal field, the ESA from the <sup>3</sup>P<sub>0</sub> upper laser level to the 4f5d configuration should not take place, at least in the visible region [26]. In 2012, Marzahl et al. [16] demonstrated an optically pumped semiconductor laser (OPSL) pumped Pr:LMA laser, yielding a maximum output power of 63.7 mW at 729.1 nm with slope efficiency of 12%. However, visible laser based on Pr:LMA crystal pumped by blue laser diodes has never been reported, to the best of our knowledge. In this paper, we have successfully grown a Pr:LMA crystal by using the Czochralski method. Furthermore, pumping with a 444 nm laser diode, laser operation of the Pr:LMA crystal in continuous-wave regime has been investigated.

## 2. Experiments

### 2.1. Crystal growth

The Pr:LMA crystal was grown using the Czochralski method from an iridium crucible heated by middle-frequency inducing generator under an atmosphere of high-purity N<sub>2</sub>. According to the formula Pr<sub>0.03</sub>La<sub>0.97</sub>MgAl<sub>11</sub>O<sub>19</sub>, the 99.999% grade raw materials of La<sub>2</sub>O<sub>3</sub>, MgO, Al<sub>2</sub>O<sub>3</sub> and Pr<sub>6</sub>O<sub>11</sub> were weighted. In consideration of the fact that

\* Corresponding author.

\*\* Corresponding author.

E-mail addresses: [xdxu79@jsnu.edu.cn](mailto:xdxu79@jsnu.edu.cn) (X. Xu), [xujun@mail.shcnc.ac.cn](mailto:xujun@mail.shcnc.ac.cn) (J. Xu).

the  $\text{La}_2\text{O}_3$  powder can absorb water rapidly from the air [27], the  $\text{La}_2\text{O}_3$  powder was heated and placed in a dry condition. After the compounds were ground and mixed, they were pressed into pieces, and heated to  $1300\text{ }^\circ\text{C}$  for 24 h in the air. The charge was then loaded into an iridium crucible for crystal growth. A seed with a  $\langle 100 \rangle$  orientation was chosen to obtain a high quality crystal. The crystal was grown at a pulling rate of  $0.8\text{ mm/h}$  and a rotation rate of  $10\text{--}30\text{ rpm}$ . After growth, the crystal was cooled to room temperature slowly for more than 60 h.

## 2.2. Spectra measurements

Samples for spectroscopic measurements were cut from the as-grown Pr:LMA crystal, and the surfaces perpendicular to the  $\langle 100 \rangle$  growth axis were polished. Room temperature polarized absorption spectra were measured with a UV–VIS–NIR spectrophotometer (Model Cary-5000, Varian, USA) at room temperature. The fluorescence spectra and the decay curve at  $643\text{ nm}$  were recorded by using Edinburgh Instruments FLS980 spectrophotometer under  $444\text{ nm}$  excitation.

## 2.3. Laser experiments

Laser experiments were carried out at green, orange, red and deep red with the following setup schematically shown in Fig. 1. Finally, green and orange laser emissions have failed to oscillate, while red and deep red laser operation have been successfully demonstrated. The pump source is an InGaN blue diode laser with maximum output power of about  $2\text{ W}$  and emitting wavelength of about  $444\text{ nm}$ . The pump beam was focused by an aspherical plane-convex lens with focal length of  $50\text{ mm}$ . The laser resonator was a two-mirror nearly hemispherical configuration with resonator length of about  $50\text{ mm}$ . For laser oscillations at red and deep red as achieved in the present experiments, two input mirrors (IMs) were used with transmissions of about  $95\%$  (for red) and  $85\%$  (for deep red) at pump wavelength. Moreover, the red IM has a transmission of about  $50\%$  at deep red, while the deep red IM has a transmission of about  $18\%$  at red, which ensures single-wavelength oscillation occurrence. At the two laser wavelengths, the two IMs have high reflections of more than  $99.9\%$ . Several output couplers (OCs) were used to explore the best laser performance with different transmissions and all these OCs have curvature radii of  $50\text{ mm}$ . For both laser oscillations (red and deep red), two OCs were used subsequently with transmissions of about  $0.3\%$  and  $0.9\%$  for red as well as  $1.2\%$  and  $3.3\%$  for deep red.

The laser gain medium is a  $3\text{ at.}\%$  doped Pr:LMA crystal cut along a crystalline axis. Its dimensions are  $3 \times 3 \times 10\text{ mm}^3$  ( $10\text{ mm}$  in thickness along the cavity axis). The crystal mounted just after the IM was protected from thermal fracture by a circular water system with temperature set at  $14\text{ }^\circ\text{C}$ .

## 3. Results and discussions

The room temperature polarized absorption spectra of Pr:LMA crystal in a range from  $400$  to  $2500\text{ nm}$  are presented in Fig. 2. The observed absorption bands are assigned to  $\text{Pr}^{3+}$  transitions from the  $^3\text{H}_4$  ground state to  $^3\text{P}_2$ ,  $^3\text{P}_1 + ^1\text{I}_6$ ,  $^3\text{P}_0$ ,  $^1\text{D}_2$ ,  $^1\text{G}_4$ ,  $^3\text{F}_4 + ^3\text{F}_3$ ,  $^3\text{F}_2$ , and  $^3\text{H}_6$

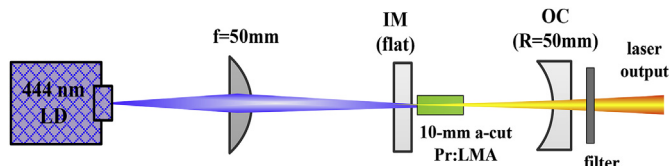


Fig. 1. The schematic of blue-diode-pumped continuous-wave a-cut Pr:LMA lasers. (For interpretation of the references to colour in this figure legend, the reader is referred to the Web version of this article.)

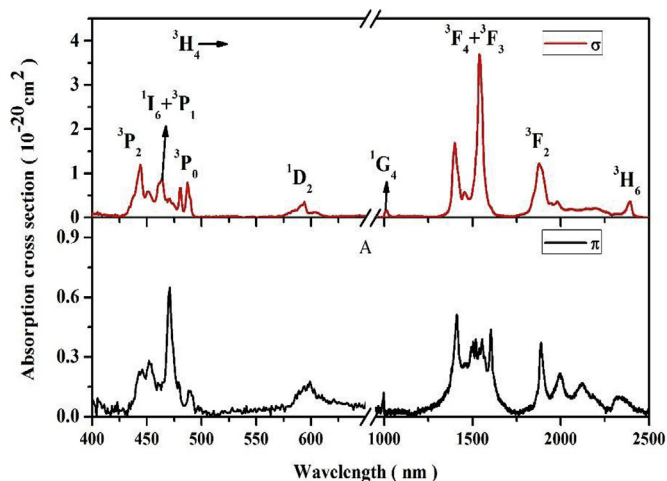


Fig. 2. Polarized absorption spectra of Pr:LMA crystal.

excited states, respectively. The peak absorption cross sections were calculated to be  $1.2 \times 10^{-20}\text{ cm}^2$  for  $\sigma$  polarization at  $444\text{ nm}$  and  $0.65 \times 10^{-20}\text{ cm}^2$  for  $\pi$  polarization at  $471\text{ nm}$ , respectively, with full width at half maximum (FWHM) of  $9.0$  and  $5.5\text{ nm}$ . The peak cross section is much lower than the value of  $1.6 \times 10^{-20}\text{ cm}^2$  at  $443.8\text{ nm}$  reported for Pr:LMA crystal [16], but is comparable with that of Pr:CaIO ( $1.1 \times 10^{-20}\text{ cm}^2$  at  $444.6\text{ nm}$  [18]), Pr:ASL ( $1.3 \times 10^{-20}\text{ cm}^2$  at  $444\text{ nm}$  [19]) and Pr:SRA crystal ( $1.3 \times 10^{-20}\text{ cm}^2$  at  $444.5\text{ nm}$  [21]). The peak located at  $444\text{ nm}$  is suitable for commercially InGaN available pump sources and a relatively large FWHM permits high conversion efficiency when pumped by InGaN laser diode.

The polarized fluorescence spectra of Pr:LMA crystal in the range of  $450\text{--}800\text{ nm}$  under  $444\text{ nm}$  excitation are shown in Fig. 3(a). The emission bands correspond to the transitions mainly from the metastable  $^3\text{P}_0$  manifolds to the lower energy level. The stimulated emission cross sections were calculated by the Fuchtbau–Ladensburg formula [28] using the radiative lifetime of Pr:LMA crystal, as presented in Fig. 3(b). In order to obtain the radiative lifetime, the Judd–Ofelt (J–O) theory [29,30] was used to calculate the spectral parameters based on the polarized absorption spectra of Pr:LMA crystal, then the radiative lifetime of the  $^3\text{P}_0$  emitting level of  $\text{Pr}^{3+}$  ions in LMA crystal was determined to be  $38.5\text{ }\mu\text{s}$ . The highest emission cross sections at  $488\text{ nm}$  (cyan),  $625\text{ nm}$  (orange),  $647\text{ nm}$  (red) and  $728\text{ nm}$  (deep red) were calculated to be  $5.6 \times 10^{-20}$ ,  $3.7 \times 10^{-20}$ ,  $2.3 \times 10^{-20}$  and  $3.3 \times 10^{-20}\text{ cm}^2$  for  $\sigma$  polarization, respectively. The values of emission cross sections are comparable with those of Pr:LMA crystal [16]. The FWHM of the emission band centered at  $488\text{ nm}$ ,  $625\text{ nm}$ ,  $647\text{ nm}$  and  $728\text{ nm}$  was calculated to be  $5.5\text{ nm}$ ,  $11.0\text{ nm}$ ,  $6.6\text{ nm}$  and  $8.5\text{ nm}$  for  $\sigma$  polarization, respectively, which indicates that the tunable laser operation and/or the generation of ultrashort pulses by mode locking might be achieved.

Fig. 4 shows the room temperature decay curve of the  $^3\text{P}_0$  excited state under  $444\text{ nm}$  excitation. The measured decay curve shows singly exponential decaying behavior. The fluorescence lifetime of the  $^3\text{P}_0$  level of  $\text{Pr}^{3+}$  was determined to be  $34.5\text{ }\mu\text{s}$ , which is comparable with that of  $2\%$  Pr:ASL ( $38\text{ }\mu\text{s}$  [19]) and  $4\%$  Pr:ASL ( $33\text{ }\mu\text{s}$  [19]). The results indicate that Pr:LMA crystal could be very promising for visible laser generation.

Fig. 5 shows results of the blue diode-pumped continuous-wave Pr:LMA lasers at deep red. Using the  $1.2\%$  OC, a maximum output power up to  $30.2\text{ mW}$  was achieved with laser threshold of about  $300\text{ mW}$  of absorbed power, which leads to a slope efficiency of about  $11.2\%$ . Using the  $3.3\%$  OC, the threshold reasonably increased to about  $350\text{ mW}$ , while the maximum output power was about  $24.3\text{ mW}$  with slope efficiency of about  $11.4\%$ . The main factor restricting the power

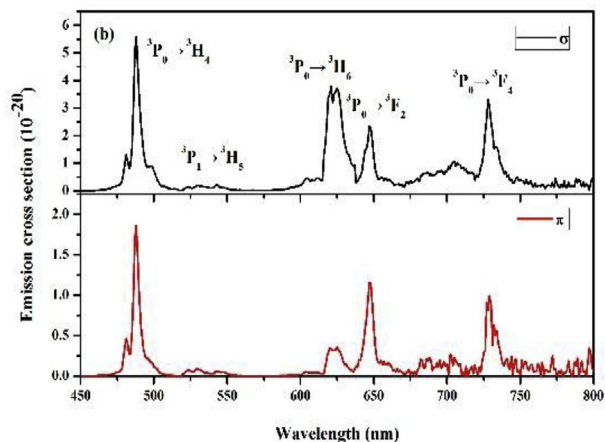
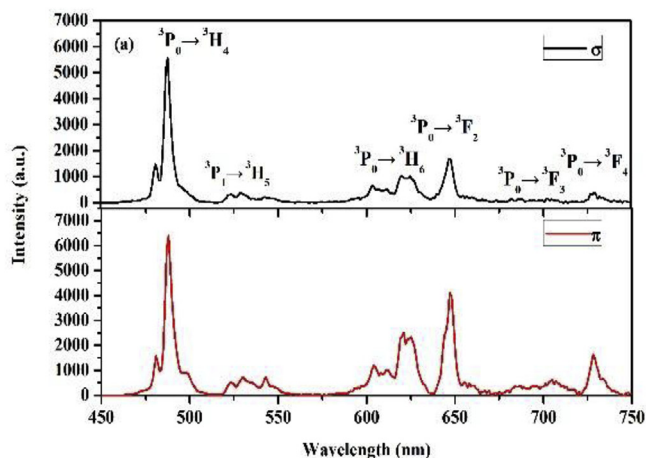


Fig. 3. (a) Polarized fluorescence spectra of Pr:LMA crystal in the range of 450–800 nm; (b) the polarized emission cross sections of Pr:LMA crystal.

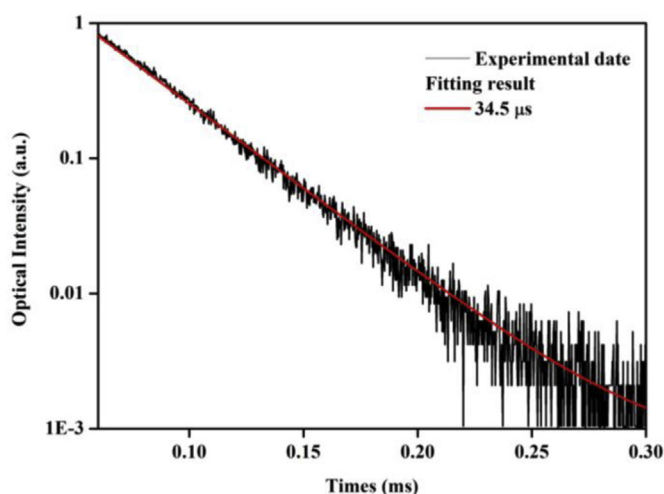


Fig. 4. The decay curve of the  $^3P_0$  level of Pr:LMA crystal.

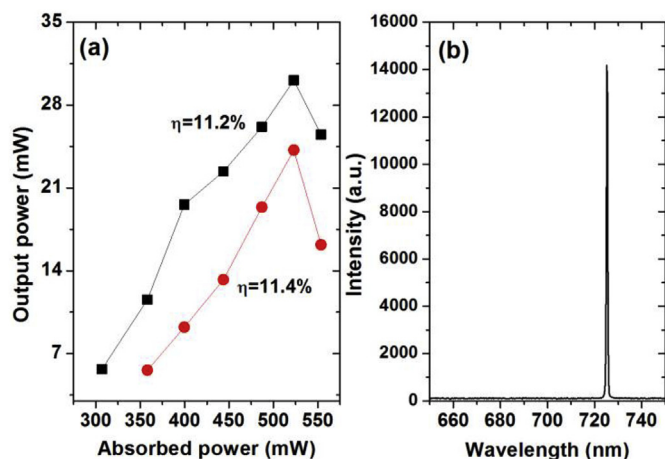


Fig. 5. (a) The dependence of output power on absorbed power and (b) the corresponding laser spectrum peaking at 725.15 nm.

scaling to higher level is the obvious saturations of the output powers for the two OCs and output power rollover can be clearly observed when the absorbed power exceeded about 530 mW, as shown in Fig. 5(a). Fig. 5(b) shows a typical laser spectrum of the present deep red emission with a peak wavelength at 725.15 nm.

Fig. 6(a) shows the dependence of output power on absorbed power

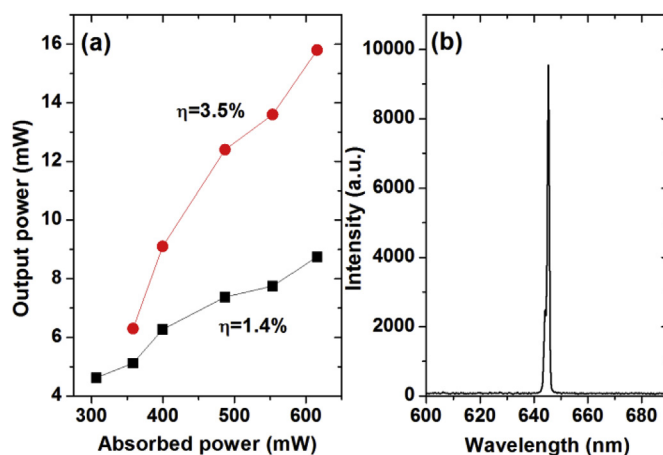


Fig. 6. (a) The dependence of output power on absorbed power and (b) the corresponding laser spectrum peaking at 645.27 nm.

of the blue diode-pumped continuous-wave Pr:LMA lasers at red. Using the 0.3% OC, a maximum output power reached about 9 mW with threshold of about 300 mW and slope efficiency of about 1.4%. The maximum output power increased to about 16 mW with slope efficiency of about 3.5%. The typical laser spectrum is shown in Fig. 6(b) with peak wavelength of about 645.27 nm. It should be pointed that for the 725 nm laser obvious rollover of output power can be observed while the rollover phenomenon is not so obvious for 645 nm laser. The output power saturation should be mainly ascribed to thermally induced lensing effect inside the Pr:LMA crystal. Relatively, the 725 nm laser suffers severer thermal effect than the 645 nm laser because of a larger quantum defect of the 725-nm laser than the 645-nm laser.

Since the Pr:LMA crystal is uniaxial, like Pr:YLF, the two laser emissions at red and deep red were also checked to be both linearly polarized, as expected. It should be pointed out that the present lasers at about 645 and 725 nm indeed provide new linearly polarized sources at these specific wavelengths, which cannot be provided by other  $Pr^{3+}$ -doped laser sources.

#### 4. Conclusion

In summary, a Pr:LMA crystal was grown by the Czochralski method. The polarized absorption spectra, emission spectra and fluorescence time of Pr:LMA crystal at room temperature were investigated. A number of material parameters relevant to laser operation were determined. The radiative and luminescence lifetimes of  $^3P_0$  level were 38.5  $\mu$ s and 34.5  $\mu$ s, respectively. The maximum emission cross sections

at 488 nm, 625 nm, 647 nm and 728 nm were calculated to be  $5.6 \times 10^{-20}$ ,  $3.7 \times 10^{-20}$ ,  $2.3 \times 10^{-20}$  and  $3.3 \times 10^{-20} \text{ cm}^2$  for  $\sigma$  polarization, respectively. Continuous-wave operation of the Pr:LMA laser pumped by a 444 nm blue diode laser have been demonstrated at red and deep red wavelengths. For red laser at about 645 nm, the maximum output power reached 16 mW with slope efficiency of about 3.5%, while for deep red laser at about 725 nm the maximum output power was about 30 mW with slope efficiency of about 11.2%. The present experiment results could be improved by optimizing the quality of the laser crystal on the one hand. On the other hand, the Pr:LMA crystal was experimentally found to have a strong thermal effect. Therefore, in the near future, power scaling could also be achieved by a better thermal management.

#### Declaration of interests

None.

#### Acknowledgements

This work is partially supported by the National Key Research and Development Program of China (No. 2016YFB0701002), National Natural Science Foundation of China (No. 61621001, 61605069), Principal fund of Xiamen University (20720180082) and The International Collaborative Laboratory of 2D Materials for Optoelectronics Science and Technology, Shenzhen University (2DMOST2018026).

#### References

- [1] C. Krankel, D.-T. Marzahl, F. Moglia, G. Huber, P.W. Metz, Out of the blue: semiconductor laser pumped visible rare-earth doped lasers, *Laser Photon. Rev.* 10 (2016) 548–568.
- [2] D.-T. Marzahl, F. Reichert, P.W. Metz, M. Fechner, N.-O. Hansen, G. Huber, Efficient laser operation of diode-pumped  $\text{Pr}^{3+}$ ,  $\text{Mg}^{2+}$ : $\text{SrAl}_2\text{O}_9$ , *Appl. Phys. B* 116 (2014) 109–114.
- [3] B. Xu, P. Camy, J. Doualan, Z.P. Cai, R. Moncorgé, Visible laser operation of  $\text{Pr}^{3+}$ -doped fluoride crystals pumped by a 469 nm blue laser, *Optic Express* 19 (2011) 1191–1197.
- [4] B. Liu, J.J. Shi, Q.G. Wang, H.L. Tang, J.F. Liu, H.Y. Zhao, D.Z. Li, J. Liu, X.D. Xu, Z.S. Wang, J. Xu, Crystal growth, polarized spectroscopy and Judd-Ofelt analysis of Pr:YAlO<sub>3</sub>, *J. Lumin.* 196 (2018) 76–80.
- [5] A. Sottile, E. Damiano, M. Tonelli, Diode-pumped laser operation of  $\text{Pr}^{3+}$ :Ba( $\text{Y}_{0.8}\text{Lu}_{0.2}$ )<sub>2</sub>F<sub>8</sub> in the visible region, *Opt. Lett.* 41 (2016) 5555–5558.
- [6] Z. Liu, Z.P. Cai, S.L. Huang, C.H. Zeng, Z.Y. Meng, Y.K. Bu, Z.Q. Luo, B. Xu, H.Y. Xu, C.C. Ye, F. Starecki, P. Camy, R. Moncorgé, Diode-pumped  $\text{Pr}^{3+}$ :LiYF<sub>4</sub> continuous-wave deep red laser at 698 nm, *J. Opt. Soc. Am. B* 30 (2013) 302–305.
- [7] M. Demesh, D.-T. Marzahl, A. Yasukevich, V. Kisel, G. Huber, N. Kuleshov, C. Krankel, Passively Q-switched Pr:YLF laser with a  $\text{Co}^{2+}$ : $\text{MgAl}_2\text{O}_4$  saturable absorber, *Opt. Lett.* 42 (2017) 4687–4690.
- [8] Y.X. Zhang, S.X. Wang, A.D. Lieto, G.L. Yu, H.H. Yu, H.J. Zhang, M. Tonelli, X.G. Xu, J.Y. Wang, Temperature-dependent fluorescence properties and diode-pumped deep red laser performance of Pr:LiGdF<sub>4</sub> crystal, *Chin. Phys. Lett.* 32 (2015) 054210.
- [9] A. Sottile, Z.H. Zhang, S. Veronesi, D. Parisi, A.D. Lieto, M. Tonelli, Visible laser operation in a  $\text{Pr}^{3+}$ :LiLuF<sub>4</sub> monocrySTALLINE fiber grown by the micro-pulling-down method, *Opt. Mater. Express* 6 (2016) 1964–1972.
- [10] B. Xu, F. Starecki, D. Pabceuf, P. Camy, J.L. Doualan, Z.P. Cai, A. Braud, R. Moncorgé, Ph Goldner, F. Bretenaker, Red and orange laser operation of Pr:KYF<sub>4</sub> pumped by a Nd:YAG/LBO laser at 469.1nm and a InGaN laser diode at 444nm, *Optic Express* 21 (2013) 5567–5574.
- [11] J. Shu, E. Damiano, A. Sottile, Z.H. Zhang, M. Tonelli, Growth by the  $\mu$ -PD method and visible laser operation of a single-crystal fiber of  $\text{Pr}^{3+}$ :KY<sub>3</sub>F<sub>10</sub>, *Crystals* 7 (2017) 200.
- [12] D. Pabceuf, O. Mhibik, F. Bretenaker, P. Goldner, D. Parisi, M. Tonelli, Diode-pumped Pr:BaY<sub>2</sub>F<sub>8</sub> continuous-wave orange laser, *Opt. Lett.* 36 (2011) 280–282.
- [13] F. Reichert, F. Moglia, D.-T. Marzahl, P. Metz, M. Fechner, N.-O. Hansen, G. Huber, Diode pumped laser operation and spectroscopy of  $\text{Pr}^{3+}$ :LaF<sub>3</sub>, *Optic Express* 20 (2012) 20387–20395.
- [14] H. Yu, D.P. Jiang, F. Tang, L.B. Su, S.Y. Luo, X.G. Yan, B. Xu, Z.P. Cai, J.Y. Wang, Q.W. Ju, J. Xu, Enhanced photoluminescence and initial red laser operation in Pr:CaF<sub>2</sub> crystal via co-doping  $\text{Gd}^{3+}$  ions, *Mater. Lett.* 206 (2017) 140–142.
- [15] M. Fibrich, J. Šulc, H. Jelínková, Pr:YAlO<sub>3</sub> laser generation in the green spectral range, *Opt. Lett.* 38 (2013) 5024–5027.
- [16] D.-T. Marzahl, F. Reichert, M. Fechner, N.-O. Hansen, G. Huber, Laser operation and spectroscopy of  $\text{Pr}^{3+}$ :LaMgAl<sub>11</sub>O<sub>19</sub>, 5th EPS-QEOD EUROPHOTON Conference, 2012 paper ThP3.
- [17] F. Reichert, D.T. Marzahl, P. Metz, M. Fechner, N.-O. Hansen, G. Huber, Efficient laser operation of  $\text{Pr}^{3+}$ ,  $\text{Mg}^{2+}$ : $\text{SrAl}_2\text{O}_9$ , *Opt. Lett.* 37 (2012) 4889–4891.
- [18] F. Reichert, D.T. Marzahl, G. Huber, Spectroscopic characterization and laser performance of Pr,Mg:CaAl<sub>12</sub>O<sub>19</sub>, *J. Opt. Soc. Am. B* 31 (2014) 349–354.
- [19] S. Sattayaporn, P. Loiseau, G. Aka, D.-T. Marzahl, C. Krankel, Crystal growth, spectroscopy and laser performances of  $\text{Pr}^{3+}$ :Sr<sub>0.7</sub>La<sub>0.3</sub>Mg<sub>0.3</sub>Al<sub>11.7</sub>O<sub>19</sub> (Pr:ASL), *Optic Express* 26 (2018) 1278–1289.
- [20] L.D. Merkle, B. Zandi, R. Moncorgé, Y. Guyot, H.R. Verdun, B. McIntosh, Spectroscopy and laser operation of Pr,Mg:SrAl<sub>12</sub>O<sub>19</sub>, *J. Appl. Phys.* 79 (1996) 1849–1856.
- [21] M. Fechner, F. Reichert, N.-O. Hansen, K. Petermann, G. Huber, Crystal growth, spectroscopy, and diode pumped laser performance of Pr,Mg:SrAl<sub>12</sub>O<sub>19</sub>, *Appl. Phys. B* 102 (2011) 731–735.
- [22] H.R. Verdun, D.E. Wortman, C.A. Morrison, J.L. Bradshaw, Optical properties of Nd<sup>3+</sup> in single crystal SrAl<sub>12</sub>O<sub>19</sub>, *Opt. Mater.* 7 (1997) 117–128.
- [23] C. Gheorghe, L. Gheorghe, A. Achim, S. Hau, R.D. Avram, G. Stanciu, Optical properties of Sm<sup>3+</sup> doped strontium hexa-aluminate single crystals, *J. Alloy. Comp.* 622 (2015) 296–302.
- [24] G. Aka, D. Vivien, V. Lupei, Site-selective 900 nm quasi-three-level laser emission in Nd-doped strontium lanthanum aluminate, *Appl. Phys. Lett.* 85 (2004) 2685–2687.
- [25] R. Collongues, A.M. Lejus, J. Théry, D. Vivien, Crystal growth and characterization of new laser materials, *J. Cryst. Growth* 128 (1993) 986–990.
- [26] A.M. Srivastava, W.W. Beers, Luminescence of  $\text{Pr}^{3+}$  in SrAl<sub>12</sub>O<sub>19</sub>: observation of two photon luminescence in oxide lattice, *J. Lumin.* 71 (1997) 285–290.
- [27] P. Xu, C.T. Xia, J.Q. Di, X.D. Xu, Q.L. Sai, L.L. Wang, Growth and optical properties of Co,Nd:LaMgAl<sub>11</sub>O<sub>19</sub>, *J. Cryst. Growth* 361 (2012) 11–15.
- [28] B. Aull H. Jenssen, Vibronic interactions in Nd:YAG resulting in nonreciprocity of absorption and stimulated emission cross sections, *IEEE J. Quant. Electron.* 18 (1982) 925–930.
- [29] B.R. Judd, Optical absorption intensities of rare-earth ions, *Phys. Rev.* 127 (1962) 750–761.
- [30] G.S. Ofelt, Intensities of crystal spectra of rare-earth ions, *J. Chem. Phys.* 37 (1962) 511–520.